

# Molecular Composition and Volatility of Nucleated Particles from $\alpha$ -Pinene Oxidation between $-50\text{ }^{\circ}\text{C}$ and $+25\text{ }^{\circ}\text{C}$

Qing Ye,<sup>†,‡</sup> Mingyi Wang,<sup>†,‡</sup> Victoria Hofbauer,<sup>†</sup> Dominik Stolzenburg,<sup>‡</sup> Dexian Chen,<sup>†,‡</sup> Meredith Schervish,<sup>†</sup> Alexander Vogel,<sup>§,¶</sup> Roy L. Mauldin,<sup>†,||</sup> Rima Baalbaki,<sup>⊥</sup> Sophia Brilke,<sup>‡</sup> Lubna Dada,<sup>⊥</sup> António Dias,<sup>#</sup> Jonathan Duplissy,<sup>@,△,⊥</sup> Imad El Haddad,<sup>∇,‡</sup> Henning Finkenzeller,<sup>††,‡‡</sup> Lukas Fischer,<sup>¶,⊥</sup> Xucheng He,<sup>⊥</sup> Changhyuk Kim,<sup>§§,|||</sup> Andreas Kürten,<sup>§</sup> Houssni Lamkaddam,<sup>∇</sup> Chuan Ping Lee,<sup>∇</sup> Katrianne Lehtipalo,<sup>⊥,⊥⊥</sup> Markus Leiminger,<sup>¶,¶</sup> Hanna E. Manninen,<sup>¶</sup> Ruby Marten,<sup>∇</sup> Bernhard Mentler,<sup>¶,¶</sup> Eva Partoll,<sup>¶,¶</sup> Tuukka Petäjä,<sup>⊥</sup> Matti Rissanen,<sup>⊥,‡</sup> Siegfried Schobesberger,<sup>##</sup> Simone Schuchmann,<sup>¶</sup> Mario Simon,<sup>§</sup> Yee Jun Tham,<sup>⊥</sup> Miguel Vazquez-Pufleau,<sup>‡</sup> Andrea C. Wagner,<sup>§</sup> Yonghong Wang,<sup>⊥</sup> Yusheng Wu,<sup>⊥</sup> Mao Xiao,<sup>∇</sup> Urs Baltensperger,<sup>∇</sup> Joachim Curtius,<sup>§</sup> Richard Flagan,<sup>§§</sup> Jasper Kirkby,<sup>¶,@@</sup> Markku Kulmala,<sup>@,△,△,△,∇,∇,∇</sup> Rainer Volkamer,<sup>††,‡‡</sup> Paul M. Winkler,<sup>‡</sup> Douglas Worsnop,<sup>†††</sup> and Neil M. Donahue\*,<sup>†,‡</sup>

<sup>†</sup>Center for Atmospheric Particle Studies, Carnegie Mellon University, Pittsburgh, Pennsylvania 15213, United States

<sup>‡</sup>Faculty of Physics, University of Vienna, Boltzmanngasse 5, 1090 Vienna, Austria

<sup>¶</sup>CERN, CH-1211 Geneva, Switzerland

<sup>§</sup>Institute for Atmospheric and Environmental Sciences, Goethe University Frankfurt, 60438, Frankfurt am Main, Germany

<sup>||</sup>Department of Oceanic and Atmospheric Science, University of Colorado Boulder, Boulder, Colorado 80309, United States

<sup>⊥</sup>Institute for Atmospheric and Earth System Research/Physics, Faculty of Science, University of Helsinki, 00014 Helsinki, Finland

<sup>#</sup>CENTRA SIM, Faculdade de Ciências, Universidade de Lisboa, Ed. C8, Campo Grande, 1749-016 Lisboa, Portugal

<sup>@</sup>Institute for Atmospheric and Earth System Research, Faculty of Science, University of Helsinki, 00014 Helsinki, Finland

<sup>△</sup>Helsinki Institute of Physics, University of Helsinki, 00014 Helsinki, Finland

<sup>∇</sup>Laboratory of Atmospheric Chemistry, Paul Scherrer Institute, 5232 Villigen, Switzerland

<sup>††</sup>Department of Chemistry, University of Colorado Boulder, Boulder, Colorado 80309, United States

<sup>‡‡</sup>Cooperative Institute for Research in Environmental Sciences (CIRES), Boulder, Colorado 80309, United States

<sup>¶¶</sup>Institute for Ion Physics and Applied Physics, University of Innsbruck, 6020 Innsbruck, Austria

<sup>§§</sup>Division of Chemistry and Chemical Engineering, California Institute of Technology, Pasadena, California 91125, United States

<sup>|||</sup>Department of Environmental Engineering, Pusan National University, 46241 Busan, Republic of Korea

<sup>⊥⊥</sup>Finnish Meteorological Institute, Erik Palménin aukio 1, 00560 Helsinki, Finland

<sup>##</sup>Department of Applied Physics, University of Eastern Finland, PO Box 1627, 70211 Kuopio, Finland

<sup>@@</sup>Goethe University Frankfurt, 60438, Frankfurt am Main, Germany

<sup>△△</sup>Joint International Research Laboratory of Atmospheric and Earth System Sciences, Nanjing University, 210023 Nanjing, China

<sup>∇∇∇</sup>Aerosol and Haze Laboratory, Beijing Advanced Innovation Center for Soft Matter Science and Engineering, Beijing University of Chemical Technology, 100029 Beijing, China

<sup>†††</sup>Aerodyne Research Inc., Billerica, Massachusetts 01821, United States

## Supporting Information

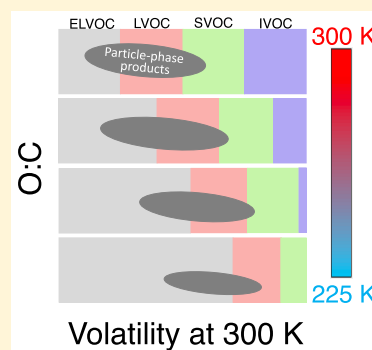
Received: May 31, 2019

Revised: September 20, 2019

Accepted: September 25, 2019

Published: September 25, 2019

**ABSTRACT:** We use a real-time temperature-programmed desorption chemical-ionization mass spectrometer (FIGAERO–CIMS) to measure particle-phase composition and volatility of nucleated particles, studying pure  $\alpha$ -pinene oxidation over a wide temperature range ( $-50\text{ }^{\circ}\text{C}$  to  $+25\text{ }^{\circ}\text{C}$ ) in the CLOUD chamber at CERN. Highly oxygenated organic molecules are much more abundant in particles formed at higher temperatures, shifting the compounds toward higher O/C and lower intrinsic (300 K) volatility. We find that pure biogenic nucleation and growth depends only weakly on temperature. This is because the positive temperature dependence of degree of oxidation (and polarity) and the negative temperature dependence of volatility counteract each other. Unlike prior work that relied on estimated volatility, we directly measure volatility via calibrated temperature-programmed desorption. Our particle-phase measurements are consistent with gas-phase results and indicate that during new-particle formation from  $\alpha$ -pinene oxidation, gas-phase chemistry directly determines the properties of materials in the condensed phase. We now have consistency between measured gas-phase product concentrations, product volatility, measured and modeled growth rates, and the particle composition over most temperatures found in the troposphere.



## INTRODUCTION

Atmospheric new-particle formation contributes up to half of the global cloud condensation nuclei (CCN) number concentration.<sup>1–3</sup> Important processes include formation of molecular clusters, stabilization where the rate of growth greatly exceeds any evaporation, and finally, growth to CCN size (50–100 nm diameter) with sufficient speed to avoid coagulation loss.<sup>4–6</sup> However, the sensitivities of the CCN budget to the mechanisms and rates of new-particle formation and growth are highly uncertain. Accurate representation and parametrization of new-particle formation for different environmental conditions in models remains a critical challenge in predicting climate forcing from aerosol indirect effects.<sup>1,7–9</sup>

Biogenic volatile organic compounds (VOC) dominate total VOC concentrations across the globe, especially in clean or moderately polluted environments.<sup>10,11</sup> Monoterpenes comprise a major fraction of biogenic VOCs, and low-volatility organic compounds from monoterpene oxidation play an essential role in new-particle formation.<sup>12,13</sup> However, until quite recently, the chemical mechanism governing formation of organic vapors that nucleate or drive condensational growth of extremely small particles (smaller than 10 nm diameter) has been unclear. Peroxy radical ( $\text{RO}_2$ ) auto-oxidation and subsequent fast association (“dimerization”) of peroxy radicals in the gas phase has emerged as a major formation pathway of highly oxygenated organic molecules (HOMs)<sup>14–18</sup> with (extremely) low vapor pressures that participate in nucleation<sup>12</sup> and initial particle growth.<sup>19</sup>

However, several questions remain unanswered. First, there is a long-standing question whether particle growth via organic condensation is rate limited by gas-phase production of low-volatility products or by reactive uptake of more volatile products followed by condensed-phase chemistry forming low-volatility products in the particle phase (glyoxal being a canonical example).<sup>20–22</sup> Second, the temperature dependence of condensable product formation (and thus secondary organic aerosol yields) remains uncertain and could depend strongly on whether condensation is rate limited by gas-phase oxidation or condensed-phase chemistry.

Quantum chemical calculations confirm that the unimolecular H atom transfers within monoterpene-derived peroxy radicals have an activation energy on the order of  $20\text{ kcal mol}^{-1}$ .<sup>23,24</sup> At warmer temperatures, auto-oxidation may outpace bimolecular termination reactions and generate products with high oxygen content and thus lower vapor pressures. At lower temperatures, due to the high energy barriers, auto-oxidation is expected to

significantly slow down compared to the barrierless termination reactions; this will suppress the yield of highly oxygenated organic compounds. In addition to influencing auto-oxidation and the formation of HOMs, the lowering of temperature also reduces saturation vapor pressures, increases saturation ratios for the same production rates, and thus provides more condensable materials to contribute to nucleation and particle growth. The trade-off between these two significant temperature effects highlights a challenge in predicting new-particle formation in environments ranging from the warm tropical surface to the outflow regions of deep-convective clouds. It also highlights the strong need to obtain full experimental closure on the temperature dependent mechanisms responsible for this process.

## BACKGROUND

Previously, Stolzenburg et al. 2018<sup>25</sup> and Frege et al. 2018<sup>26</sup> measured the composition of gas-phase products and small charged clusters during new-particle formation from  $\alpha$ -pinene over a range of temperatures in the Cosmic Leaving Outdoor Droplets (CLOUD) facility at CERN. Frege et al. 2018<sup>26</sup> used an atmospheric pressure interface time-of-flight mass spectrometer (APi-ToF) to measure naturally charged ions, showing that low temperature ( $-25\text{ }^{\circ}\text{C}$ ) favors formation of products with lower oxygen content and lower molecular weight compared to products formed at high temperature ( $+25\text{ }^{\circ}\text{C}$ ). Stolzenburg et al. 2018<sup>25</sup> combined measurements from a proton-transfer-reaction mass spectrometer and a nitrate anion chemical ionization mass spectrometer (CIMS) to measure neutral gas-phase species with a wide range of polarity and volatility, finding that products formed at low temperature ( $-25\text{ }^{\circ}\text{C}$ ) have a higher room-temperature saturation vapor pressure than products formed at high temperature ( $+25\text{ }^{\circ}\text{C}$ ). Volatility in this case was estimated using a simple composition-volatility relationship.<sup>25,27</sup> Further, they modeled particle growth using a dynamical Volatility Basis Set (VBS) to treat both the curvature (Kelvin) and condensed-phase mixing (Raoult) effects on condensed-phase activity and were able to quantitatively reproduce particle growth rates derived from a suite of microphysical instruments.

However, due to the lack of detailed composition and volatility measurements of the particles following new-particle formation and condensational growth, it is not known whether measurements of particle-phase composition will confirm our understanding of the temperature dependence of the gas-phase chemistry, or whether the particle composition will show signs of

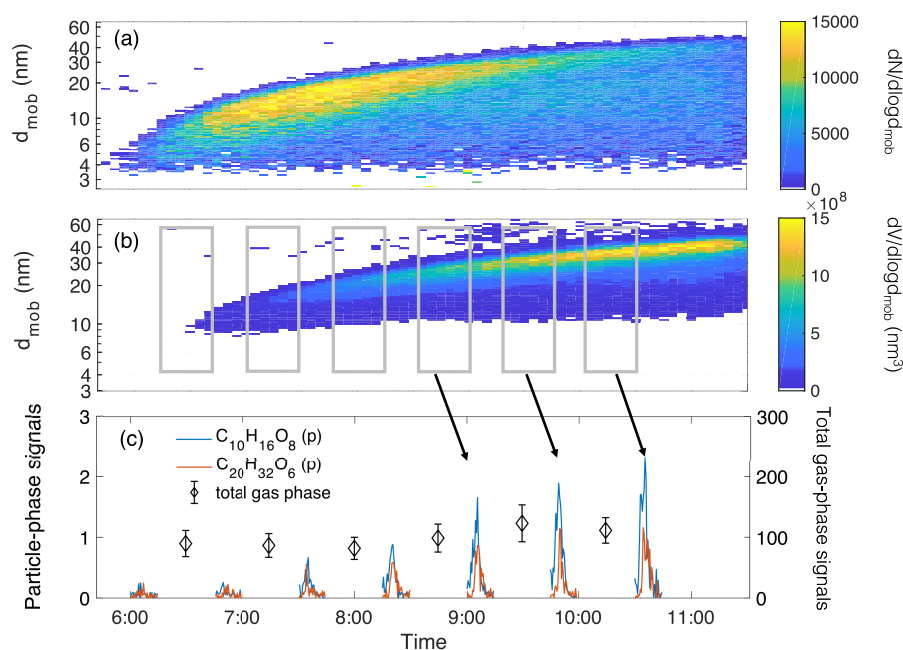


**Figure 1.** Example experiment performed with 600 pptv  $\alpha$ -pinene and 40 ppbv ozone in the chamber at  $-50\text{ }^{\circ}\text{C}$  and 90% RH. Panels a and b are merged size-distribution data measured by a nano-SMPS and a long-SMPS for the new-particle formation event. Panel a shows the number distribution and panel b shows the volume distribution. Time periods in the gray squares in panel b are the particle collection intervals (30 min each) for the FIGAERO. The arrows indicate the corresponding signals during subsequent thermal-desorption cycles (panel c). Each thermal desorption cycle lasts 15 min. The signals of a representative monomer ( $\text{C}_{10}\text{H}_{16}\text{O}_8$  (p)) and dimer ( $\text{C}_{20}\text{H}_{32}\text{O}_6$  (p)) product rise with total particle volume but remain roughly proportional, consistent with a constant particle composition. The gas phase was in a steady state during the experiment, as confirmed by the total gas-phase signal shown as black diamonds averaged over each gas-phase collection interval measured by the  $\text{I}^-$  CIMS. The constant gas phase signal and initially low filter desorption signal confirms that the FIGAERO filter signal represents the particle-phase composition.

subsequent condensed-phase chemistry. To answer those questions, here, we present real-time particle-phase composition measurements from a series of CLOUD experiments of new-particle formation from pure  $\alpha$ -pinene oxidation over a wide temperature range ( $-50$  to  $+25\text{ }^{\circ}\text{C}$ ) with atmospherically relevant precursor concentrations. We use a Filter Inlet for Gases and Aerosols (FIGAERO) thermal desorption inlet on an iodide CIMS. We first describe the overall response of the instrument to new-particle formation events in the CLOUD chamber, then characterize the broad set of identified products, and finally show the progressive evolution of composition and volatility of the products versus temperature in the two-dimensional volatility basis set.<sup>27</sup> Using direct temperature-programmed desorption, we infer volatility during new-particle formation and confirm that covalently bound dimers of  $\alpha$ -pinene oxidation products are present in newly formed particles. Our objective is to investigate whether full closure exists between the observed gas-phase species and concentrations, the observed particle growth rates, and the observed condensed-phase composition at all temperatures.

## MATERIALS AND METHODS

**CLOUD Chamber.** The CLOUD chamber at CERN is a  $26.1\text{ m}^3$  stainless steel chamber with precisely controlled temperature, humidity, and constituent gases. It is fed as a continuously stirred tank reactor with a flow of synthetic air formed by mixing vapor from liquid nitrogen and liquid oxygen storage tanks. VOC gases are diluted to the required concentration with pure air before entering into the chamber. The temperature in the chamber is controlled to a precision of  $\pm 0.1\text{ }^{\circ}\text{C}$  over a broad range from  $-65$  to  $30\text{ }^{\circ}\text{C}$ , and the chamber is mixed rapidly by inductively coupled fans mounted at the top and bottom. Ions

are controlled in three states (“neutral”, “galactic cosmic ray”, and “beam”) via a switchable high-voltage clearing field and regulated exposure to a  $3.5\text{ GeV } \pi^+$  beam from the CERN proton-synchrotron. A suite of real-time gas- and particle-phase instruments sample the chamber simultaneously, collectively establishing a flushing time of approximately 1.5 h. More details can be found in Kirkby et al. 2011<sup>28</sup> and Duplissy et al. 2016.<sup>29</sup>

Results presented here are from  $\alpha$ -pinene oxidation experiments during the CLOUD-12 campaign in Fall 2017 under galactic cosmic ray conditions at four different temperatures:  $-50\text{ }^{\circ}\text{C}$ ,  $-25\text{ }^{\circ}\text{C}$ ,  $+5\text{ }^{\circ}\text{C}$ , and  $+25\text{ }^{\circ}\text{C}$ . The  $\alpha$ -pinene concentration was 600 pptv for experiments at  $-50\text{ }^{\circ}\text{C}$ ,  $+5\text{ }^{\circ}\text{C}$ , and  $+25\text{ }^{\circ}\text{C}$  and 1200 pptv for the experiment at  $-25\text{ }^{\circ}\text{C}$  (experiment at 600 pptv is not available). We held ozone at a constant 40 ppbv and performed all experiments in the dark, and no hydroxyl radical scavenger was used. The chamber’s relative humidity (RH) was 90% for experiments at  $-50\text{ }^{\circ}\text{C}$  and  $-25\text{ }^{\circ}\text{C}$  and 38% for experiments at  $+5\text{ }^{\circ}\text{C}$  and  $+25\text{ }^{\circ}\text{C}$ . We do not expect the difference in humidity to significantly influence our results as  $\text{RO}_2$ -derived HOM formation shows limited RH dependence.<sup>30</sup> In the chamber, the background concentration of nitrogen oxides was in the sub pptv range and the background sulfuric acid concentration was lower than  $5 \times 10^4\text{ cm}^{-3}$ .<sup>28</sup> For these experiments, we added no nitrogen oxides or sulfur dioxide into the chamber and so these results represent  $\text{NO}_x$ -free “pure biogenic” organic conditions.

**FIGAERO Chemical Ionization Mass Spectrometer.** We used a chemical ionization mass spectrometer (CIMS) with a Filter Inlet for Gas and AEROSol (FIGAERO) (Aerodyne Research Inc. & ToFwerk AG) to measure the nucleated particles from  $\alpha$ -pinene oxidation. The FIGAERO–CIMS, which has a sensitivity on the  $\text{pg m}^{-3}$  level, has been described in detail in



Lopez-Hilfiker et al. 2014.<sup>31</sup> In brief, it measures gas-phase compounds while collecting particles on a Teflon filter in the inlet at a flow rate of 8 L per minute. After particle collection, the FIGAERO switches to a particle thermal desorption mode in which the filter is bathed in heated nitrogen carrier gas ranging from room temperature to about 160 °C following a temperature program. Because the entire filter manifold is made of Teflon and thus has very low thermal conductivity, it responds rapidly to the changing carrier-gas temperature. The thermally desorbed compounds from the collected particles subsequently flow into an ion–molecule reactor and are measured by the downstream CIMS. Figure S1 shows examples of thermal-desorption profiles of representative products identified from the experiments here. The gas-phase sampling/particle collection time in our experiments was 30 min, and the thermal desorption mode lasted for 15 min before the instrument returned to the gas sampling and particle collection mode. Here, we focus largely on the particle-mode data.

We used iodide as the reagent ion as it can cluster effectively with low-volatility organic compounds.<sup>32</sup> We produced iodide ions by passing methyl iodide from a permeation source over a <sup>210</sup>Po foil. The long time-of-flight (LTOF) mass spectrometer has a mass resolving power of up to 12000 (Tofwerk AG). We collected data at 1 Hz and averaged them to 0.1 Hz for post processing.

The temperature of the maximum desorption signal ( $T_{\text{max}}$ ) during the particle mode correlates with vapor pressure and vaporization enthalpy,<sup>31,33</sup> provided that compounds do not thermally decompose.<sup>34</sup> We performed volatility calibrations by manually depositing an aliquot of a mixture of several known pure organic acids and fitting the  $1/T_{\text{max}}$  (in K) of each calibrant with their subcooled liquid vapor pressure. We calibrated with the filter starting at room temperature and show representative data in the Supporting Information. We use the calibration curve to estimate the gas-phase saturation concentration of all the measured compounds by correlating  $1/T_{\text{max}}$  with their saturation vapor pressure.

## RESULTS AND DISCUSSION

**FIGAEROCIMS Measurements of New-Particle Formation.** We first present an example of a new-particle formation event in the CLOUD chamber from pure  $\alpha$ -pinene oxidation and show the corresponding FIGAERO particle-phase signals. In this event, the  $\alpha$ -pinene concentration was 600 pptv and the chamber temperature was  $-50$  °C. In Figure 1a, we show the particle number size distribution combining measurements from a nano-SMPS (TSI, Inc.) and a custom-made long-SMPS. This is a so-called “banana” with time on the  $x$ -axis, mobility diameter on the (log)  $y$ -axis, and the number size distribution shown via colors; the nucleation event in this case occurred somewhat before the earliest time shown, and subsequent condensation drove growth from roughly 3 to 30 nm over 4 h, made evident by the leading (upper) edge. This growth rate of  $8 \text{ nm h}^{-1}$  is typical of atmospheric new-particle formation events<sup>5</sup> and indicates that condensable vapors in the experiment were similar to those typical of the atmosphere. Because the FIGAERO provides a bulk mass measurement, we show the corresponding particle volume distribution in Figure 1b. We highlight the particle collection periods in the FIGAERO inlet with gray boxes (30 min each). For example, when we collected particles between 8:30 and 9:00, the leading edge was just over 20 nm, and data from the corresponding thermal desorption cycle appear between 9:00 and 9:15.

In Figure 1c, we show representative data from the particle desorption cycles for a monomer product,  $\text{C}_{10}\text{H}_{16}\text{O}_8\text{I}^-$ , and a dimer product,  $\text{C}_{20}\text{H}_{32}\text{O}_6\text{I}^-$ . Here, we define monomer products as ions containing 10 or fewer carbon atoms and dimer products as ions containing 11 to 20 carbon atoms. When there is sufficient mass loading (after 8:00 in this case), the peak signal for the dimer product always appears after the monomer product because it has a lower vapor pressure. As the new-particle formation proceeds and particles grow to larger sizes, signals of both the monomer and dimer products in the particle phase increase correspondingly in proportion to the particle volume.

We examined the size-dependence of total oxygen to carbon elemental ratio (O/C) during a new particle-formation event and found no observable change in O/C versus particle size. There is thus no evidence from the FIGAERO data that the particle composition changes significantly during an event. This may be because the time resolution (45 min) of our data is not fine enough to capture the very beginning of the particle growth period where the Kelvin effect is most critical<sup>19,25</sup> or simply that the signal-to-noise for particles smaller than 10 nm is insufficient to resolve any composition differences. For the results we show in the rest of this paper, we use the data from the last cycle for each experiment in order to maximize the signal-to-noise.

Our signal generally consists of a background that is nearly independent of temperature overlain by a well-defined thermal desorption peak, as shown in Figure S4. To separate these, we fit a linear background, as shown, and interpret the peak area of the temperature-dependent peak above this background as the signal due to particles collected on the filter during the sampling cycle. As we show in Figure S3, the sum of peak areas of all identified products in a sampling cycle is proportional to the corresponding average SMPS mass. Further, during nucleation events with a constant HOM vapor concentration (such as the event shown in Figure 1), the total signals of the first FIGAERO cycle in which there are barely any particles in the chamber is generally well under 8% of maximum FIGAERO cycle. For our quantitative analysis, we use the signal from the end of each event, with maximum suspended volume; we thus conclude that this signal is almost entirely due to collected particles, with little or negligible interference from adsorbed vapors on the filter.

In Figure S5a, we correlate the FIGAERO signals with known mass concentration of a mixture of organic acids as shown. In Figure S5b, we correlate the total particle-phase mass measured by the FIGAERO–CIMS and the average integrated particle concentration during particle collection cycles under all temperatures, as measured by the SMPS. The total particle mass from the FIGAERO correlates well with the SMPS mass, with an  $r^2$  of 0.89. We find a ratio of 1.6 between the inferred total mass based on filter calibrations (presuming a constant sensitivity of the  $\text{I}^-$  chemical ionization) and the inferred mass based on the SMPS mass assuming a particle density of  $1.4 \text{ g cm}^{-3}$ . We have observed correspondingly good correlation between the integrated FIGAERO signal and total particle volume during a number of CLOUD campaigns.<sup>35</sup> This indicates that the overall sensitivity of the FIGAERO–CIMS to particle loading is consistent across different experiments in our studies and that we are recovering a large fraction, if not all, of the total available mass.

**Measured Products from FIGAERO–CIMS.** In Figure 2, we show a representative mass-defect plot for particle-phase constituents from  $\alpha$ -pinene oxidation at  $+5$  °C. We show mass-defect plots for all temperatures in Figure S6 in the Supporting

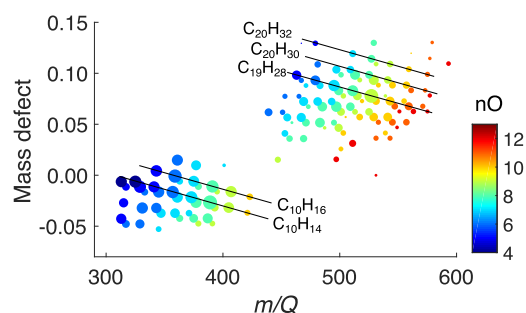


**Figure 2.** Mass-defect plot for nucleated particles at +5 °C. Marker size corresponds to the square root of the ion signals, while color indicates number of oxygen atoms, as shown. We show the ions attached with  $\text{I}^-$ . The band between 300 and 450 Th is the “monomer” band of (largely)  $\text{C}_{10}$  species, while the band between 450 and 600 Th is the “dimer” band of (largely)  $\text{C}_{20}$  species. Each (slightly tilted) row corresponds to species with progressively more oxygen atoms, whereas each column corresponds to species with progressively more hydrogen atoms (almost entirely with an even hydrogen number).

**Information.** We are able to clearly measure the monomers ( $\text{C}_{7-10}$  compounds) and dimers ( $\text{C}_{14-20}$  compounds) in the particle phase at all temperatures in our experiments. Here, we only show iodide adducts ( $\text{C}_x\text{H}_y\text{O}_z\text{I}^-$ ), although a small portion of the detected ions underwent iodide declustering.<sup>32</sup> Due to the extremely low level of  $\text{NO}_x$  in the chamber (sub pptv), we do not observe any signals from nitrogen containing species, consistent with  $\text{NO}_x$ -free conditions.

In Figure 2, we color code the symbols by oxygen number. In the monomer mass range, detected compounds show  $4 \leq n_{\text{O}} \leq 10$  at 5 °C. In the dimer mass range, the oxygen number varies from  $5 \leq n_{\text{O}} \leq 13$ . Products with higher oxygen content may also exist, as gas-phase products with up to 18 oxygens are detected by the nitrate-chemical ionization mass spectrometer deployed in the same campaign (manuscript in preparation). But the signals of these products in the particle phase may be too low in our instruments to produce a reliable signal above the background. As shown in Figure S6, as the temperature drops, the products shift progressively toward lower oxygen content in both the monomer and the dimer bands. This is consistent with gas-phase observations from CLOUD-10 and CLOUD-11<sup>25,26</sup> that the rate of auto-oxidation is lower during new-particle formation at lower temperature, producing less oxidized products at low temperature than at high temperature. In addition, lower temperature enhances condensation of compounds with higher room-temperature saturation vapor pressures, which may be less oxygenated. For instance, at +25 °C, for the  $\text{C}_{10}\text{H}_y\text{O}_z$  series, the lowest oxygen content measured in the particle phase is  $\text{O}_6$ , while at −25 °C and −50 °C, the lowest oxygen content is  $\text{O}_3$ , as shown in Figure S6. We shall discuss this more in the next section.

As Figure 2 shows, we detected many dimer products in the thermal desorption data. This confirms that dimers from  $\alpha$ -pinene oxidation are covalently bounded, likely from  $\text{RO}_2 + \text{RO}_2$  association reactions,<sup>36</sup> as they thermally desorbed without evident fragmentation at temperatures as high as 130 °C in our instrument (also see Figure S1). We did not detect any products in the trimer ( $\text{C}_{30}$ ) or tetramer ( $\text{C}_{40}$ ) mass ranges, though these species were observed as naturally occurring ions by the APi-ToF-CIMS in prior CLOUD experiments.<sup>26</sup> This is consistent with these higher mass ions being molecular clusters of covalently bound monomers and dimers that appear only as

monomers and dimers in the bulk particle thermal desorption data.

**Volatility Distributions of Nucleated Particles versus Temperature.** In Figure 3, we present the condensed-phase

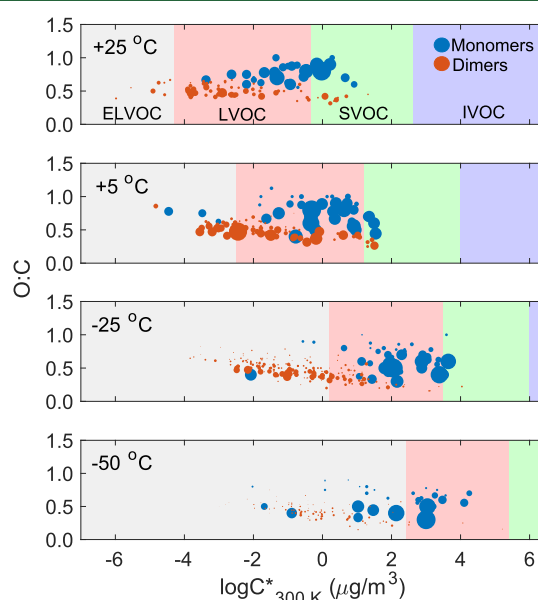


**Figure 3.** FIGAERO particle-phase data for  $\alpha$ -pinene oxidation projected onto a 2D-VBS for the nucleated particles at CLOUD temperatures (from top to bottom) of +25 °C, +5 °C, −25 °C, and −50 °C. Symbol colors differentiate monomers and dimers, and symbol sizes are ion signals normalized by the highest signal in each temperature. The calibrated assessment of the volatility as  $C^*$  (300 K) of the desorbed compounds is shown in the  $x$  axis. From left to right, the broad, colored bands in the background are volatility classes of extremely low-volatility organic compounds (ELVOC), low-volatility organic compounds (LVOC), semivolatile organic compounds (SVOC), and intermediate-volatility organic compounds (IVOC). These classes are defined by actual volatility ( $C^*$  (T)) and so shift with temperature according to the Clausius–Clapeyron equation.

constituents at different temperatures within the two-dimensional volatility basis set (2D-VBS) introduced by Donahue et al. 2011.<sup>27</sup> The  $x$ -axis is the log of saturation concentration ( $C_{300\text{ K}}^*$ ) experimentally estimated using the thermal desorption profile measured at 300 K described in the Supporting Information. We report volatility as  $C^*$  (and not  $C^\circ$ ) because our observations are over mixtures and thus implicitly include activity coefficients. The  $y$ -axis is the observed oxygen to carbon ratio, O/C. Every data point is normalized by the largest signal at each temperature, and the size of each data point signifies the signal level. The different broad colored bands in the background represent the volatility classes of extremely low-volatility organic compounds (ELVOC), low-volatility organic compounds (LVOC), semivolatile organic compounds (SVOC), and intermediate-volatility organic compounds (IVOC). We shift the volatility classes for the lower temperature experiments using the Clausius–Clapeyron relation and the enthalpy of evaporation in Donahue et al. 2011<sup>27</sup> and Epstein and Donahue 2009<sup>37</sup> because the classes are fundamentally associated with atmospheric saturation ratios. Details of this calculation are in the Supporting Information. We also show that the products aggregated into a 1D-VBS ( $C^*$  only) at four temperatures in Figure S7 of the Supporting Information.

The counterbalancing effects of oxidation and temperature are evident in Figure 3, where to a great extent, the condensed-phase products remain in the LVOC range, with a tail extending into the ELVOC range. At +25 °C, most of the products have a 300 K saturation concentration lower than 1  $\mu\text{g m}^{-3}$ . As temperature decreases, there is a progressive shift of both the monomer and dimer products toward higher 300 K (intrinsic) saturation concentration and toward lower O/C. This is consistent with reduced formation of HOMs as observed by previous gas-phase measurements.<sup>25,26</sup> This also reflects the temperature effects on the saturation vapor pressure. Therefore, the suppressed formation of compounds with lower volatility is compensated by the shift of the volatility classes at lower temperatures, indicated by the shifted colored bands in Figure 3. For example, a compound with  $\log C^* = 2$  at 300 K is an SVOC at +25 °C and +5 °C, but it is an LVOC at −25 °C and an ELVOC at −50 °C. This supports the roughly constant particle growth below 10 nm observed across a wide range of temperatures by Stolzenburg et al. 2018.<sup>25</sup>

During low-temperature experiments, we used insulation to maintain the temperature between the chamber and the instrument sampling/filter system. Still there may have been loss of higher-volatility compounds during the low-temperature experiments. Therefore, our low-temperature measurements should be a lower bound of the signals from the actual collected material. This could be why the −50 °C distribution does not extend through the LVOC region, as the molecules at the LVOC-SVOC boundary are quite volatile at room temperature.

Further, some decomposition occurred during thermal desorption, and some observed monomers (blue symbols) are actually products of dehydration<sup>33</sup> or decomposition of dimers;<sup>38</sup> these have volatilities (indicated by peak signal temperatures) much lower than most of other monomer products as shown in the volatility space in Figure 3 and instead appear within the dimer region. Despite these caveats, the evolution in both the volatility and the O/C direction in the 2D-VBS as a function of temperature is clear, and most of the identified products have volatilities based on peak thermal desorption temperature that are consistent with our broad estimates of their vapor pressures based on their molecular formulas.<sup>27</sup>

The volatilities used in prior nucleation and growth experiments on  $\alpha$ -pinene oxidation were estimated based on composition.<sup>19,25</sup> The volatilities we show here in Figure 3 are directly measured based on peak desorption temperature. However, the experimental conditions were similar during different CLOUD campaigns. On the basis of measured vapor concentrations and estimated volatility distributions, Stolzenburg et al. 2018 were able to quantitatively reproduce the observed size-dependent growth rates at −25 °C, +5 °C, and +25 °C (they did not reach −50 °C) using a dynamical VBS model. Their results indicated that the condensing vapors remained just within the LVOC envelope (approximately 1 order of magnitude to the left of the LVOC-SVOC dividing line at all temperatures). Here, we show direct confirmation of this result at the corresponding temperatures, though our particle phase composition measurements with direct measurement of the volatility suggest that the demarcation is closer to the LVOC-SVOC dividing line. This represents a strong agreement within approximately 1 order of magnitude in volatility (over a range of many orders of magnitude).

Our particle-phase observations show that the molecules condensing to drive particle growth are progressively more

oxidized at elevated temperature and also that there is a significant presence of covalently bound dimer species. This confirms that the rate-limiting step for particle growth in this case is the gas-phase formation of HOMs (rather than subsequent particle phase chemistry) and is consistent with the rate-limiting step for nucleation, which is the gas-phase formation of dimers from RO<sub>2</sub> reactions, at least for  $T \geq -25$  °C. At −50 °C, the products are dominated by products with relatively low signals of auto-oxidation products, relatively low O/C, and low dimer formation; however, the temperature is so low that even the mildly oxidized products are essentially ELVOCs capable of both nucleation and growth. That in turn is consistent with very high overall secondary organic aerosol mass yields previously reported for  $\alpha$ -pinene oxidation at very low temperature.<sup>39,40</sup> It also implies that at high altitudes, even slightly oxidized compounds (e.g., first-generation products without auto-oxidation) may condense to facilitate new particle formation and growth.<sup>41</sup>

With all results taken together, our study shows that lower temperature reduces the production of HOMs but at the same time promotes the condensation of less oxidized vapors to facilitate particle formation and growth. Our condensed-phase volatility measurements are consistent with volatility distributions from growth rate calculation using gas-phase observations. In summary, the volatility distributions are consistent to within an order of magnitude (out of nearly 10) and the growth rates are consistent to within ~30%.<sup>25</sup> Further, we confirm a significant population of covalently bound dimer species that survive thermal decomposition; these are thought to be critical for “pure biogenic” nucleation, though subsequent growth is driven by monomer HOM species. Our results indicate that for the  $\alpha$ -pinene oxidation system, at least in the early stage of particle formation and growth under the typical loadings and conditions that were used in the CLOUD chamber, gas-phase chemistry, instead of condensed-phase or heterogeneous reactions that occur after the condensation of low- or semivolatile organics, is the dominant driver of the properties of biogenic SOA particles.

## ■ ASSOCIATED CONTENT

### § Supporting Information

The Supporting Information is available free of charge on the ACS Publications website at DOI: 10.1021/acs.est.9b03265.

Volatility measurements in the FIGAERO–CIMS, mass measurements in the FIGAERO–CIMS, shifts of volatility classes as a function of temperature and supporting figure (PDF)

## ■ AUTHOR INFORMATION

### Corresponding Author

\*E-mail: nmd@andrew.cmu.edu.

### ORCID

Qing Ye: 0000-0003-3797-8988

Mingyi Wang: 0000-0001-5782-2513

Dexian Chen: 0000-0001-6963-5205

Alexander Vogel: 0000-0002-1293-6370

Jonathan Duplissy: 0000-0001-8819-0264

Imad El Haddad: 0000-0002-2461-7238

Lukas Fischer: 0000-0002-3141-9088

Matti Rissanen: 0000-0003-0463-8098

Neil M. Donahue: 0000-0003-3054-2364



## Notes

The authors declare no competing financial interest.

## ACKNOWLEDGMENTS

We thank the European Organization for Nuclear Research (CERN) for supporting CLOUD with important technical and financial resources. This research has received funding from the U.S. National Science Foundation under grants AGS-1801574, AGS-1801897, AGS-1649147, and AGS-1602086; the EC Horizon 2020 Programme (Marie-Sklodowska-Curie Innovative Training Network “CLOUD-MOTION” No. 764991); European Union Horizon 2020 programme MC-COFUND Grant 665779; German Federal Ministry of Education and Research (No. 01LK1601A); ERC-Consolidator Grant NANO-DYNAMITE 616075; Horizon 2020 Marie Skłodowska-Curie Grant 656994 (Nano-CAVa); ERC Advanced “ATM-GP” grant No. 227463; and the Swiss National Science Foundation Project 20FI20\_159851, 200021\_169090, 200020\_172602 and 20FI20\_172622. The FIGAERO-CIMS was supported by an MRI grant for the U.S. NSF AGS-1531284 as well as the Wallace Research Foundation. Q.Y. was supported by a Faculty for the Future Fellowship from the Schlumberger Foundation.

## REFERENCES

- (1) Pierce, J. R.; Adams, P. J. Uncertainty in global CCN concentrations from uncertain aerosol nucleation and primary emission rates. *Atmos. Chem. Phys.* **2009**, *9*, 1339–1356.
- (2) Merikanto, J.; Spracklen, D.; Mann, G.; Pickering, S.; Carslaw, K. Impact of nucleation on global CCN. *Atmos. Chem. Phys.* **2009**, *9*, 8601–8616.
- (3) Spracklen, D. V.; Carslaw, K. S.; Kulmala, M.; Kerminen, V.-M.; Sihto, S.-L.; Riipinen, I.; Merikanto, J.; Mann, G. W.; Chipperfield, M. P.; Wiedensohler, A.; Birmili, W.; Lihavainen, H. Contribution of particle formation to global cloud condensation nuclei concentrations. *Geophys. Res. Lett.* **2008**, *35*, 06808.
- (4) McMurry, P.; Friedlander, S. New particle formation in the presence of an aerosol. *Atmos. Environ.* (1967-1989) **1979**, *13*, 1635–1651.
- (5) Riipinen, I.; Yli-Juuti, T.; Pierce, J. R.; Petäjä, T.; Worsnop, D. R.; Kulmala, M.; Donahue, N. M. The contribution of organics to atmospheric nanoparticle growth. *Nat. Geosci.* **2012**, *5*, 453–458.
- (6) Kulmala, M.; Kontkanen, J.; Junninen, H.; Lehtipalo, K.; Manninen, H. E.; Nieminen, T.; Petäjä, T.; Sipilä, M.; Schobesberger, S.; Rantala, P.; Franchin, A.; Jokinen, T.; Järvinen, E.; Aijälä, M.; Kangasluoma, J.; Hakala, J.; Aalto, P.; Paasonen, P.; Mikkilä, J.; Vanhanen, J.; Aalto, J.; Hakola, H.; Makkonen, U.; Ruuskanen, T.; Mauldin, R. L.; Duplissy, J.; Vehkamäki, H.; Bäck, J.; Kortelainen, K. E.; Riipinen, I.; Kurtén, T.; Johnson, M.; Smith, J. N.; Ehn, M.; Mentel, T. F.; Lehtinen, K. E. J.; Laaksonen, A.; Kerminen, V.; Worsnop, D. Direct observations of atmospheric aerosol nucleation. *Science* **2013**, *339*, 943–946.
- (7) Wang, M.; Penner, J. Aerosol indirect forcing in a global model with particle nucleation. *Atmos. Chem. Phys.* **2009**, *9*, 239–260.
- (8) Kazil, J.; Stier, P.; Zhang, K.; Quaas, J.; Kinne, S.; O’donnell, D.; Rast, S.; Esch, M.; Ferrachat, S.; Lohmann, U.; Feichter, J. Aerosol nucleation and its role for clouds and Earth’s radiative forcing in the aerosol-climate model ECHAM5-HAM. *Atmos. Chem. Phys.* **2010**, *10*, 10733–10752.
- (9) Gordon, H.; Sengupta, K.; Rap, A.; Duplissy, J.; Frege, C.; Williamson, C.; Heinritzi, M.; Simon, M.; Yan, C.; Almeida, J.; Tröstl, J.; Nieminen, T.; Ortega, I. K.; Wagner, R.; Dunne, E.; Adamov, A.; Amorim, A.; Bernhammer, A.; Bianchi, F.; Breitenlechner, M.; Brilke, S.; Chen, X.; Craven, J.; Dias, A.; Ehrhart, S.; Fischer, L.; Flagan, R. C.; Franchin, A.; Fuchs, C.; Guida, R.; Hakala, J.; Hoyle, C.; Jokinen, T.; Junninen, H.; Kangasluoma, J.; Kim, J.; Kirkby, J.; Krapf, M.; Kurten, A.; Laaksonen, A.; Lehtipalo, K.; Makhmutov, V.; Mathot, S.; Molteni, U.; Monks, S.; Onnela, A.; Perakyla, O.; Piel, F.; Petäjä, T.; Praplan, A.; Pringle, K.; Richards, N. A. D.; Rissanen, M.; Rondo, L.; Sarnela, N.; Schobesberger, S.; Scott, C.; Seinfeld, J. H.; Sharma, S.; Sipilä, M.; Steiner, G.; Stozhkov, Y.; Stratmann, F.; Tome, A.; Virtanen, A.; Vogel, A.; Wagner, A. C.; Wagner, P. E.; Weingartner, E.; Wimmer, D.; Winkler, P. M.; Ye, P.; Zhang, X.; Hansel, A.; Dommen, J.; Donahue, N. M.; Worsnop, D. R.; Baltensperger, U.; Kulmala, M.; Curtius, J.; Carslaw, K. S. Reduced anthropogenic aerosol radiative forcing caused by biogenic new particle formation. *Proc. Natl. Acad. Sci. U. S. A.* **2016**, *113*, 12053–12058.
- (10) Guenther, A.; Karl, T.; Harley, P.; Wiedinmyer, C.; Palmer, P. I.; Geron, C. Estimates of global terrestrial isoprene emissions using MEGAN (Model of Emissions of Gases and Aerosols from Nature). *Atmos. Chem. Phys.* **2006**, *6*, 3181–3210.
- (11) Chung, S. H. Global distribution and climate forcing of carbonaceous aerosols. *J. Geophys. Res.* **2002**, *107*, 14–33, DOI: 10.1029/2001JD001397.
- (12) Kirkby, J.; Duplissy, J.; Sengupta, K.; Frege, C.; Gordon, H.; Williamson, C.; Heinritzi, M.; Simon, M.; Yan, C.; Almeida, J.; Tröstl, J.; Nieminen, T.; Ortega, I.; Wagner, R.; Adamov, A.; Amorim, A.; Bernhammer, A.; Bianchi, F.; Breitenlechner, M.; Brilke, S.; Chen, X.; Craven, J.; Dias, A.; Ehrhart, S.; Flagan, R. C.; Franchin, A.; Fuchs, C.; Guida, R.; Hakala, J.; Hoyle, C. R.; Jokinen, T.; Junninen, H.; Kangasluoma, J.; Kim, J.; Krapf, M.; Kurten, A.; Laaksonen, A.; Lehtipalo, K.; Makhmutov, V.; Mathot, S.; Molteni, U.; Onnela, A.; Perakyla, O.; Piel, F.; Petäjä, T.; Praplan, A.; Pringle, K.; Rap, A.; Richards, N. A. D.; Riipinen, I.; Rissanen, M. P.; Rondo, L.; Sarnela, N.; Schobesberger, S.; Scott, C.; Seinfeld, J. H.; Sipilä, M.; Steiner, G.; Stozhkov, Y.; Stratmann, F.; Tome, A.; Virtanen, A.; Vogel, A.; Wagner, A. C.; Wagner, P. E.; Weingartner, E.; Wimmer, D.; Winkler, P. M.; Ye, P.; Zhang, X.; Hansel, A.; Dommen, J.; Donahue, N. M.; Worsnop, D. R.; Baltensperger, U.; Kulmala, M.; Carslaw, K.; Curtius, J. Ion-induced nucleation of pure biogenic particles. *Nature* **2016**, *533*, 521.
- (13) Riccobono, F.; Schobesberger, S.; Scott, C.; Dommen, J.; Ortega, I.; Rondo, L.; Almeida, J.; Amorim, A.; Bianchi, F.; Breitenlechner, M.; David, A.; Downard, A.; Dunne, E.; Duplissy, J.; Ehrhart, S.; Flagan, R. C.; Franchin, A.; Hansel, A.; Junninen, H.; Kajos, M.; Keskinen, H.; Kupc, A.; Kurten, A.; Kvashin, A. N.; Laaksonen, A.; Lehtipalo, K.; Makhmutov, V.; Mathot, S.; Nieminen, T.; Onnela, A.; Petäjä, T.; Praplan, A. P.; Santos, F. D.; Schallhart, S.; Seinfeld, J. H.; Sipilä, M.; Spracklen, D. V.; Stozhkov, Y.; Stratmann, F.; Tome, A.; Tsagkogeorgas, G.; Vaattovaara, P.; Viisanen, Y.; Vrtala, A.; Wagner, P. E.; Weingartner, E.; Wex, H.; Wimmer, D.; Carslaw, K.; Curtius, J.; Donahue, N. M.; Kirkby, J.; Kulmala, M.; Worsnop, D. R.; Baltensperger, U. Oxidation products of biogenic emissions contribute to nucleation of atmospheric particles. *Science* **2014**, *344*, 717–721.
- (14) Ehn, M.; Thornton, J. A.; Kleist, E.; Sipilä, M.; Junninen, H.; Pullinen, I.; Springer, M.; Rubach, F.; Tillmann, R.; Lee, B.; Lopez-Hilfiker, F.; Andres, S.; Acir, I.; Rissanen, M.; Jokinen, T.; Schobesberger, S.; Kangasluoma, J.; Kontkanen, J.; Nieminen, T.; Kurtén, T.; Nielsen, L. B.; Jorgensen, S.; Kjaergaard, H. G.; Canagaratna, M.; Dal Maso, M.; Berndt, T.; Petaja, T.; Wahner, A.; Kerminen, V.; Kulmala, M.; Worsnop, D. R.; Wildt, J.; Mentel, T. F. A large source of low-volatility secondary organic aerosol. *Nature* **2014**, *506*, 476–479.
- (15) Jokinen, T.; Sipilä, M.; Richters, S.; Kerminen, V.-M.; Paasonen, P.; Stratmann, F.; Worsnop, D.; Kulmala, M.; Ehn, M.; Herrmann, H.; Berndt, T. Rapid autooxidation forms highly oxidized RO<sub>2</sub> radicals in the atmosphere. *Angew. Chem., Int. Ed.* **2014**, *53*, 14596–14600.
- (16) Zhao, Y.; Thornton, J. A.; Pye, H. O. Quantitative constraints on autooxidation and dimer formation from direct probing of monoterpene-derived peroxy radical chemistry. *Proc. Natl. Acad. Sci. U. S. A.* **2018**, *115*, 12142–12147.
- (17) Jokinen, T.; Berndt, T.; Makkonen, R.; Kerminen, V.-M.; Junninen, H.; Paasonen, P.; Stratmann, F.; Herrmann, H.; Guenther, A. B.; Worsnop, D. R.; Kulmala, M.; Ehn, M.; Sipilä, M. Production of extremely low volatile organic compounds from biogenic emissions: Measured yields and atmospheric implications. *Proc. Natl. Acad. Sci. U. S. A.* **2015**, *112*, 7123.

- (18) Bianchi, F.; Kurtén, T.; Riva, M.; Mohr, C.; Rissanen, M.; Roldin, P.; Berndt, T.; Crounse, J.; Wennberg, P.; Mentel, T. F.; Wildt, J.; Junninen, H.; Jokinen, T. L.; Kulmala, M.; Worsnop, D. R.; Thornton, J. A.; Donahue, N. M.; Kjaergaard, H. G.; Ehn, M. Highly oxygenated molecules (HOM) from gas-phase autoxidation of organic peroxy radicals: A key contributor to atmospheric aerosol. *Chem. Rev.* **2019**, *119*, 3472.
- (19) Tröstl, J.; Chuang, W. K.; Gordon, H.; Heinritzi, M.; Yan, C.; Molteni, U.; Ahlm, L.; Frege, C.; Bianchi, F.; Wagner, R.; Simon, M.; Lehtipalo, K.; Williamson, C.; Craven, J. S.; Duplissy, F.; Adamov, A.; Almeida, J.; Bernhammer, A.; Breitenlechner, M.; Brilke, S.; Dias, A.; Ehrhart, S.; Flagan, F. C.; Franchin, A.; Fuchs, C.; Guida, R.; Gysel, M.; Hansel, A.; Hoyle, C. R.; Jokinen, T.; Junninen, H.; Kangasluoma, J.; Keskinen, K.; Kim, J.; Krapf, M.; Kurten, A.; Laaksonen, A.; Lawler, M.; Leiminger, M.; Mathot, S.; Möhler, O.; Nieminen, T.; Onnela, A.; Petäjä, T.; Piel, F.; Miettinen, P.; Rissanen, M. P.; Rondo, L.; Sarnela, N.; Schobesberger, S.; Sengupta, K.; Sipilä, M.; Smith, J. N.; Steiner, G.; Tome, A.; Virtanen, A.; Wagner, A. C.; Weingartner, E.; Wimmer, D.; Winkler, P. M.; Ye, P.; Carslaw, K. S.; Curtius, J.; Dommen, J.; Kirkby, J.; Kulmala, M.; Riipinen, I.; Worsnop, D. R.; Donahue, N. M.; Baltensperger, U. The role of low-volatility organic compounds in initial particle growth in the atmosphere. *Nature* **2016**, *533*, 527.
- (20) Volkamer, R.; San Martini, F.; Molina, L. T.; Salcedo, D.; Jimenez, J. L.; Molina, M. J. A missing sink for gas-phase glyoxal in Mexico City: Formation of secondary organic aerosol. *Geophys. Res. Lett.* **2007**, *34*, 19807.
- (21) Waxman, E. M.; Dzepina, K.; Ervens, B.; Lee-Taylor, J.; Aumont, B.; Jimenez, J. L.; Madronich, S.; Volkamer, R. Secondary organic aerosol formation from semi-and intermediate-volatility organic compounds and glyoxal: Relevance of O/C as a tracer for aqueous multiphase chemistry. *Geophys. Res. Lett.* **2013**, *40*, 978–982.
- (22) Chuang, W. K.; Donahue, N. M. Dynamic consideration of smog chamber experiments. *Atmos. Chem. Phys.* **2017**, *17*, 10019–10036.
- (23) Rissanen, M. P.; Kurtén, T.; Sipilä, M.; Thornton, J. A.; Kausiala, O.; Garmash, O.; Kjaergaard, H. G.; Petäjä, T.; Worsnop, D. R.; Ehn, M.; Kulmala, M. Effects of chemical complexity on the autoxidation mechanisms of endocyclic alkene ozonolysis products: From methylcyclohexenes toward understanding  $\alpha$ -pinene. *J. Phys. Chem. A* **2015**, *119*, 4633–4650.
- (24) Kurtén, T.; Rissanen, M. P.; Mackeprang, K.; Thornton, J. A.; Hyttinen, N.; Jørgensen, S.; Ehn, M.; Kjaergaard, H. G. Computational study of hydrogen shifts and ring-opening mechanisms in  $\alpha$ -pinene ozonolysis products. *J. Phys. Chem. A* **2015**, *119*, 11366–11375.
- (25) Stolzenburg, D.; Fischer, L.; Vogel, A.; Heinritzi, M.; Schervish, M.; Simon, M.; Wagner, A. C.; Dada, L.; Ahonen, L. R.; Amorim, A.; Baccarini, A.; Bauer, P. S.; Baumgartner, B.; Bergen, A.; Bianchi, F.; Breitenlechner, M.; Brilke, S.; Buenrostro Mazon, S.; Chen, D.; Dias, A.; Draper, D. C.; Duplissy, J.; El-Haddad, I.; Finkenzeller, H.; Frege, C.; Fuchs, C.; Garmash, O.; Gordon, H.; He, X.; Helm, J.; Hofbauer, V.; Hoyle, C. R.; Kim, C.; Kirkby, J.; Kontkanen, J.; Kurten, A.; Lampilahti, J.; Lawler, M.; Lehtipalo, K.; Leiminger, M.; Mai, H.; Mathot, S.; Mentler, B.; Molteni, U.; Nie, W.; Nieminen, T.; Nowak, J. B.; Ojdanic, A.; Onnela, A.; Passananti, M.; Petäjä, T.; Quelever, L.; Rissanen, M. P.; Sarnela, N.; Schallhart, S.; Tauber, C.; Tome, A.; Wagner, R.; Wang, M.; Weitz, L.; Wimmer, D.; Xiao, M.; Yan, C.; Ye, P.; Zha, Q.; Baltensperger, U.; Curtius, J.; Dommen, J.; Flagan, F. C.; Kulmala, M.; Smith, J. N.; Worsnop, D. R.; Hansel, A.; Donahue, N. M.; Winkler, P. M. Rapid growth of organic aerosol nanoparticles over a wide tropospheric temperature range. *Proc. Natl. Acad. Sci. U. S. A.* **2018**, *115*, 9122–9127.
- (26) Frege, C.; Ortega, I. K.; Rissanen, M. P.; Praplan, A. P.; Steiner, G.; Heinritzi, A.; Ahonen, L.; Amorim, A.; Bernhammer, A.; Bianchi, F.; Brilke, S.; Breitenlechner, M.; Dada, L.; Dias, A.; Duplissy, J.; Ehrhart, S.; El-Haddad, I.; Fischer, L.; Fuchs, C.; Garmash, O.; Gonin, M.; Hansel, A.; Hoyle, C. R.; Jokinen, T.; Junninen, H.; Kirkby, J.; Kurten, A.; Lehtipalo, K.; Leiminger, M.; Mauldin, R. L.; Molteni, U.; Nichman, L.; Petäjä, T.; Sarnela, N.; Schobesberger, S.; Simon, M.; Sipilä, M.; Stolzenburg, D.; Tome, A.; Vogel, A. L.; Wagner, A. C.; Wanger, R.; Xiao, M.; Yan, C.; Ye, P.; Curtius, J.; Donahue, N. M.; Flagan, R. C.; Kulmala, M.; Worsnop, D. R.; Winkler, P. M.; Dommen, J.; Baltensperger, U. Influence of temperature on the molecular composition of ions and charged clusters during pure biogenic nucleation. *Atmos. Chem. Phys.* **2018**, *18*, 65–79.
- (27) Donahue, N. M.; Epstein, S.; Pandis, S. N.; Robinson, A. L. A two-dimensional volatility basis set: 1. organic-aerosol mixing thermodynamics. *Atmos. Chem. Phys.* **2011**, *11*, 3303–3318.
- (28) Kirkby, J.; Curtius, J.; Almeida, J.; Dunne, E.; Duplissy, J.; Ehrhart, S.; Franchin, A.; Gagné, S.; Ickes, L.; Kürten, A.; Kupc, A.; Metzger, A.; Riccobono, F.; Rondo, J.; Schobesberger, S.; Tsagkogeorgas, G.; Wimmer, D.; Amorim, A.; Bianchi, F.; Breitenlechner, M.; David, A.; Dommen, J.; Downard, A.; Ehn, M.; Flagan, R. C.; Haider, A.; Hansel, A.; Hauser, D.; Jud, W.; Junninen, H.; Kreissl, F.; Kvashin, A.; Laaksonen, A.; Lehtipalo, J.; Lima, J.; Lovejoy, E.; Makhmutov, V.; Mathot, S.; Mikkilä, J.; Minginette, P.; Mogo, S.; Nieminen, T.; Onnela, A.; Pereira, P.; Petäjä, T.; Schnitzhofer, R.; Seinfeld, J. H.; Sipilä, M.; Stozhkov, Y.; Stratmann, F.; Tome, A.; Vanhanen, J.; Viisanen, Y.; Vrtala, A.; Wagner, P. E.; Walther, H.; Weingartner, E.; Wex, H.; Winkler, P. M.; Carslaw, K. S.; Worsnop, D. R.; Baltensperger, U.; Kulmala, M. Role of sulphuric acid, ammonia and galactic cosmic rays in atmospheric aerosol nucleation. *Nature* **2011**, *476*, 429–433.
- (29) Duplissy, J.; Merikanto, J.; Franchin, A.; Tsagkogeorgas, G.; Kangasluoma, J.; Wimmer, D.; Vuollekoski, H.; Schobesberger, S.; Lehtipalo, K.; Flagan, R. C.; Brus, D.; Donahue, N. M.; Vehkamäki, H.; Almeida, J.; Amorim, A.; Barmet, P.; Bianchi, F.; Breitenlechner, M.; Dunne, E.; Guida, R.; Henschel, H.; Junninen, H.; Kirkby, J.; Kurten, A.; Kupc, A.; Maattanen, A.; Makhmutov, V.; Mathot, S.; Nieminen, T.; Onnela, A.; Praplan, A. P.; Riccobono, F.; Rondo, L.; Steiner, G.; Tome, A.; Walther, H.; Baltensperger, U.; Carslaw, K. S.; Dommen, J.; Hansel, A.; Petäjä, T.; Sipilä, M.; Stratmann, F.; Vrtala, A.; Wagner, P. E.; Worsnop, D. R.; Curtius, J.; Kulmala, M. Effect of ions on sulfuric acid-water binary particle formation: 2. Experimental data and comparison with QC-normalized classical nucleation theory. *Journal of Geophysical Research: Atmospheres* **2016**, *121*, 1752–1775.
- (30) Li, X.; Chee, S.; Hao, J.; Abbatt, J. P.; Jiang, J.; Smith, J. N. Relative humidity effect on the formation of highly oxidized molecules and new particles during monoterpene oxidation. *Atmos. Chem. Phys.* **2019**, *19*, 1555–1570.
- (31) Lopez-Hilfiker, F.; Mohr, C.; Ehn, M.; Rubach, F.; Kleist, E.; Wildt, J.; Mentel, T. F.; Lutz, A.; Hallquist, M.; Worsnop, D.; Thornton, J. A. A novel method for online analysis of gas and particle composition: description and evaluation of a Filter Inlet for Gases and AEROSols (FIGAERO). *Atmos. Meas. Tech.* **2014**, *7*, 983–1001.
- (32) Lee, B. H.; Lopez-Hilfiker, F. D.; Mohr, C.; Kurtén, T.; Worsnop, D. R.; Thornton, J. A. An iodide-adduct high-resolution time-of-flight chemical-ionization mass spectrometer: Application to atmospheric inorganic and organic compounds. *Environ. Sci. Technol.* **2014**, *48*, 6309–6317.
- (33) Stark, H.; Yatavelli, R. L. N.; Thompson, S. L.; Kang, H.; Krechmer, J. E.; Kimmel, J. R.; Palm, B. B.; Hu, W.; Hayes, P. L.; Day, D. A.; Campuzano-Jost, P.; Canagaratna, M. R.; Jayne, J. T.; Worsnop, D. R.; Jimenez, J. L. Impact of thermal decomposition on thermal desorption instruments: advantage of thermogram analysis for quantifying volatility distributions of organic species. *Environ. Sci. Technol.* **2017**, *51*, 8491–8500.
- (34) Wang, M.; Yao, L.; Zheng, J.; Wang, X.; Chen, J.; Yang, X.; Worsnop, D. R.; Donahue, N. M.; Wang, L. Reactions of atmospheric particulate stabilized Criegee intermediates lead to high-molecular-weight aerosol components. *Environ. Sci. Technol.* **2016**, *50*, 5702–5710.
- (35) Wang, M.; CLOUD; Donahue, N. M. Mechanisms that control the contribution of aromatic highly oxidized multifunctional compounds (HOMs) to initial particle growth in the atmosphere. *in prep.*
- (36) Berndt, T.; Scholz, W.; Mentler, B.; Fischer, L.; Herrmann, H.; Kulmala, M.; Hansel, A. Accretion Product Formation from Self-and Cross-Reactions of RO<sub>2</sub> Radicals in the Atmosphere. *Angew. Chem., Int. Ed.* **2018**, *57*, 3820–3824.



- (37) Epstein, S. A.; Riipinen, I.; Donahue, N. M. A semiempirical correlation between enthalpy of vaporization and saturation concentration for organic aerosol. *Environ. Sci. Technol.* **2010**, *44*, 743–748.
- (38) Clafin, S. M.; Ziemann, P. J. Thermal desorption behavior of hemiacetal, acetal, ether, and ester oligomers. *Aerosol Sci. Technol.* **2019**, *53*, 473–484.
- (39) Saathoff, H.; Naumann, K.-H.; Möhler, O.; Jonsson, Å. M.; Hallquist, M.; Kiendler-Scharr, A.; Mentel, T. F.; Tillmann, R.; Schurath, U. Temperature dependence of yields of secondary organic aerosols from the ozonolysis of  $\alpha$ -pinene and limonene. *Atmos. Chem. Phys.* **2009**, *9*, 1551–1577.
- (40) Quéléver, L. L. J.; Kristensen, K.; Jensen, L.; Rosati, B.; Teiwes, R.; Daellenbach, K. R.; Peräkylä, O.; Roldin, P.; Pedersen, H. B.; Glasius, M.; Bilde, M.; Ehn, M. Effect of temperature on the formation of Highly-oxygenated Organic Molecules (HOM) from alpha-pinene ozonolysis. *Atmos. Chem. Phys. Discuss.* **2018**, *2018*, 1–29.
- (41) Murphy, B. N.; Julin, J.; Riipinen, I.; Ekman, A. M. Organic aerosol processing in tropical deep convective clouds: Development of a new model (CRM-ORG) and implications for sources of particle number. *J. Geophys. Res.: Atmos.* **2015**, *120*, 10–441.